Heat Transfer Model of Directional Solidification by LMC Process for Superalloy Casting Based on Finite Element Method

LIU CAO, DUNMING LIAO, YUZHANG LU, and TAO CHEN

With the rapid development of the aviation industry, the turbine blade, a critical component of the aeronautical engine, has come to be widely produced by liquid-metal cooling (LMC) process. A temperature- and time-dependent heat transfer coefficient was used to represent the heat convection between the shell and the cooling liquid, and an improved Monte Carlo ray-tracing approach was adopted to handle the boundary of radiation heat transfer. Unstructured mesh was used to fit the irregular shell boundary, and the heat transfer model of directional solidification by LMC process based on finite element method (FEM) was established. The concept of local matrix was here proposed to guarantee computational efficiency. The pouring experiments of directional solidification by LMC process were carried out, then simulation and experimental results were compared here. The accuracy of the heat transfer model was validated by the cooling curves and grain morphology, and the maximum relative error between simulation and experimental cooling curve was 2 pct. The withdrawal rate showed an important influence on the shape of solidification interface, and stray grain is liable to be generated on the bottom of platform at an excessive withdrawal rate.

DOI: 10.1007/s11661-016-3619-z

I. INTRODUCTION

SINGLE crystal (SX) superalloy blades are the key hot components of advanced gas turbines and aeronautical engines due to their high-temperature strength, oxidation resistance, and fatigue resistance. Directional solidification (DS) process is used to control the grain orientation strictly and eliminate grain boundaries, which contributes to the excellent comprehensive properties of SX blades.[1,2] As a conventional DS method, high-rate solidification[3,4] (HRS) has been widely adopted in the industry. During the HRS process, the shell is gradually drawn into the cooling zone, after preheating and pouring are complete. Heat radiates step by step, eventually forming the DS process. However, owing to the low thermal gradient on the solidification interface,[5] the use of HRS can lead to a series of problems, such as stray grains and freckling when casting large components.[6,7] One method of achieving high and consistent thermal gradients is the utilization of liquid-metal cooling[8–10] (LMC) process. During the process of LMC, the shell is gradually immersed in the liquid-metal coolant at a certain rate, losing heat by both conduction and convection. The cooling rate and thermal gradient were significantly better under the LMC process than under HRS,[11,12] giving LMC an obvious advantage in the manufacturing of large SX castings.[13–15]

The optimization of LMC process is difficult and costly by experimental methods, especially for the complexly shaped gas turbine blades, owing to the complicated technological parameters of solidification process. Therefore, numerical simulation is effective to optimize the technological process and also provides theoretical guidance. Napolitano *et al.*[16] evaluated a set of nickel-based superalloy SX investment castings for crystal perfection, reaching a conclusion that the appearance of stray grain on the platform is closely related to the shape of liquid/solid interface, and a higher withdrawal rate causes the curvature of liquid/solid interface increase, making stray grain appear easily on the platform. Kermanpur *et al.*[17] simulated the thermal field and the grain structure of a cored superalloy turbine blade during LMC process by commercial software ProCAST (ESI Group, Pairs, France), which were compared with experimental observation. Elliott *et al.*[18] simulated the LMC temperature field in two dimensions, concluding that heat transfer between the casting and the interior mold surface is the primary resistance in the LMC process, and heat extraction is enhanced by lowering the coolant temperature in this process. Lu *et al.*[19,20] prepared directionally solidified industry gas turbine hollow blades by high gradient LMC process, and the impact of withdrawal rate on the formation of stray grains and freckles was predicted, which was consist with the experimental observations. Yan *et al.*[21] established the mathematical models for dynamic heat radiation and convection boundary of

YUZHANG LU, Ph.D. Student, is with the Institute of Metal Research, Chinese Academy of Sciences, Shenyang 110016, Liaoning, P. R. China. Contact e-mail:luyuzhang84@163.com LIU CAO, Ph.D. Student, DUNMING LIAO, Professor, and TAO CHEN, Postdoctoral Fellow, are with the State Key Laboratory of Materials Processing and Die & Mould Technology, Huazhong University of Science and Technology (HUST), Wuhan 430074, Hubei, P. R. China.
Manuscript submitted January 20, 2016
Article published online June 29, 2016

LMC process to simulate the temperature field based on finite difference method, and described the nucleation and growth by cellular automaton (CA) method and KGT growth model.

Finite difference method[22] (FDM), finite volume method[23] (FVM), and finite element method[24] (FEM) are the three most common numerical methods used in the field of numerical simulation by casting. FDM is easy to implement, though it is only suitable for structured mesh because it cannot fit complex surface boundaries well.[25,26] FVM has definite physical meaning for conservation and can be used with unstructured mesh, but the calculation accuracy is limited.[27,28] FEM is appropriate for unstructured mesh and has a high calculation accuracy for solving thermal fields.[29,30] Considering that the irregular shell boundary is needed to be handled in numerical simulation of LMC process, it has a certain value to research the heat transfer model of DS by LMC process based on FEM.

A temperature- and time-dependent heat transfer coefficient was used to represent the heat convection between the shell and the coolant, and an improved Monte Carlo ray-tracing approach was used to handle the boundary of radiation heat transfer in this paper. Unstructured mesh was adopted to fit the irregular shell boundary. The heat transfer model of DS by LMC process based on FEM was established, and the concept of local matrix was proposed to guarantee computational efficiency. Through the work above, a temperature field numerical simulation program of DS by LMC process based on FEM was developed. The pouring experiments of DS by LMC process were carried out, then simulation and experimental results were compared, and the influence that withdrawal rate showed on the shape of solidification interface and stray grain was analyzed in this paper.

II. HEAT TRANSFER MODEL OF LMC PROCESS

A. *Governing Equations*

Heat conduction equation, which is deduced from Fourier heat equation and the law of conservation of energy, is the basic equation that describes the heat transfer process. The differential equation that the field variable $T(x, y, z, t)$ of transient temperature field in three dimensions under Cartesian coordinate system should satisfy[31] is:

$$\rho c\frac{\partial T}{\partial t}-\frac{\partial}{\partial x}\left(k_x\frac{\partial T}{\partial x}\right)-\frac{\partial}{\partial y}\left(k_y\frac{\partial T}{\partial y}\right)-\frac{\partial}{\partial z}\left(k_z\frac{\partial T}{\partial z}\right)-\rho Q=0, \quad [1]$$

where ρ is the density, kg/m^3, c is the specific heat, J/(kg K), t is the time, s, k_x, k_y, k_z are the thermal conductivities in the three principal directions, W/m/K, and Q is the inner heat source density, W/kg. In this paper, the isotropous thermal conductivity is adopted, namely $k_x = k_y = k_z$.

B. *The Boundary of Radiation Heat Transfer*

As radiation heat distributes in three-dimensional space, it needs to be discretized on the physical level, and ray tracing is needful before dealing with the boundary of radiation heat transfer. Owing to the complexity of LMC process, including the radiation baffle, the water cooling crystallizer, and the drawing motion between casting and shell, more attention must be paid to the boundary of radiation heat transfer.

The physical discretization method for the boundary of radiation heat transfer is an improved Monte Carlo ray-tracing approach[32–34] in this paper. Figure 1 shows the thinking of physical discretization that the upper hemisphere space is divided into multisubspaces, each of which is replaced by several corresponding rays, and the final location of each ray should be recorded in order to gain the element j shot by the ray and its temperature T_j. It should be made clear that the radiation energy represented by each ray is supposed to be absorbed totally by the element j, so the radiation angle factor φ_j is equal to the constant one. The subspace represented by a ray can be determined by the angle α with the X-axis, the horizontal included angle $\Delta\alpha$, the angle β with the Z-axis and the vertical included angle $\Delta\beta$. By summing the radiation energy of each subspace, the total radiation energy Q_{rad} between the surface element and the outside can be determined as:

$$Q_{\text{rad}}=\sum_{j=1}^{n}Q_j \quad [2]$$

$$Q_j=\eta_j\sigma\left(T^4-T_j^4\right)\Big/\left(\tfrac{1-\varepsilon}{\varepsilon}\cdot\tfrac{1}{S}+\tfrac{1-\varepsilon_j}{\varepsilon_j}\cdot\tfrac{1}{S_j}+\tfrac{1}{S}\right), \quad [3]$$

where n is the number of the subspaces, ε and ε_j are the surface emissivity of materials on the ray's origin and endpoint, respectively, S and S_j are the area of elements on the ray's origin and endpoint, respectively, m^2, σ is the *Stefan–Boltzmann* constant, J/(s m^2 K^4), and η_j is the radiant weight factor which is applied to express the ratio between the radiation force represented by the ray j and the total radiation force of the surface element.

According to the *Lambert* law, the radiation force of the subspace can be gotten from the integral operation, so the radiant weight factor can be determined by:

$$\eta_j=\frac{\Delta\alpha}{4\pi}\cdot[\cos(2\beta-\Delta\beta)-\cos(2\beta+\Delta\beta)] \quad [4]$$

The radiation heat transfer is applied to the surface element, so the boundary condition of radiation heat transfer can be formulated as:

$$k_x\frac{\partial T}{\partial x}n_x+k_y\frac{\partial T}{\partial y}n_y+k_z\frac{\partial T}{\partial z}n_z=-\frac{Q_{\text{rad}}}{S}, \quad [5]$$

where n_x, n_y, and n_z are the direction cosines of the surface element's exterior normal.

By substituting Eqs. [2], [3], and Eq. [4] into Eq. [5] and the linearization process, the boundary condition of radiation heat transfer can be set as:

$$k_x \frac{\partial T}{\partial x} n_x + k_y \frac{\partial T}{\partial y} n_y + k_z \frac{\partial T}{\partial z} n_z = D_0 - D_1 T, \quad [6]$$

where:

$$D_0 = \sum_{j=1}^{n} \left[\eta_j \cdot \sigma \cdot T_j^4 \Big/ \left(\frac{1}{\varepsilon} + \frac{1-\varepsilon_j}{\varepsilon_j} \cdot \frac{S}{S_j} \right) \right] + 3T_e^4 \cdot \sum_{j=1}^{n} \left[\eta_j \cdot \sigma \Big/ \left(\frac{1}{\varepsilon} + \frac{1-\varepsilon_j}{\varepsilon_j} \cdot \frac{S}{S_j} \right) \right] \quad [7]$$

$$D_1 = 4T_e^3 \cdot \sum_{j=1}^{n} \left[\eta_j \cdot \sigma \Big/ \left(\frac{1}{\varepsilon} + \frac{1-\varepsilon_j}{\varepsilon_j} \cdot \frac{S}{S_j} \right) \right] \quad [8]$$

T_e is the average temperature of surface element, K.

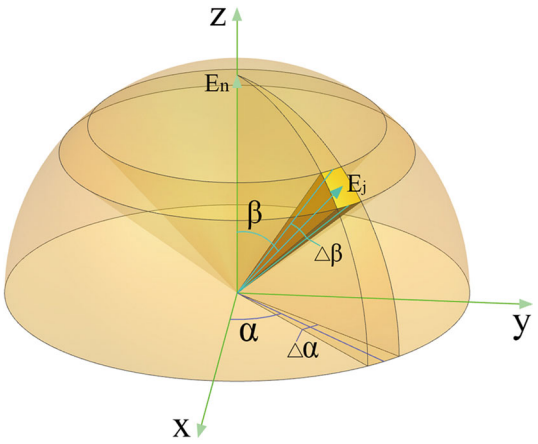

Fig. 1—The schematic diagram of physical discretization for the boundary of radiation heat transfer.[32]

C. *The Boundary of Convection Heat Transfer between Shell and Coolant*

As the shell is immersed into the liquid-metal coolant gradually in LMC process, the way of heat exchange shifts from radiation to convection in terms of the boundary condition of heat transfer. If the change process of coolant is taken into account directly during LMC process in simulation, the problem of remeshing for the 3D mesh will arise, which is difficult to implement and needs high computational cost. Therefore, a temperature- and time-dependent heat transfer coefficient[35] is used to treat the heat convection between the shell and the liquid-metal coolant in this paper.

Kutateladze *et al.*[35] researched the phenomenon of heat convection between different liquid-metal coolant and solid, and analyzed the experimental results and analytic model. Eventually, a mathematical relationship about Nusselt number (Nu), Prandtl number (Pr), and Grashof number (Gr) has been formulated as:

$$Nu = C\left(\frac{Pr^2 Gr}{1+Pr}\right)^n, \quad [9]$$

where

$$Nu = \frac{hL}{k} \quad [10]$$

$$Pr = \frac{c\mu}{k} \quad [11]$$

$$Gr = \frac{g\beta\rho^2}{\mu^2}\Delta T L^3 \quad [12]$$

When the value of Gr is low ($10^2 < Gr < 10^8$), they found that $C = 0.67$ and $n = 1/4$, whereas at higher value ($Gr > 10^8$),$C = 0.16$ and $n = 1/3$. By substituting

Table I. The Physical Parameters of Liquid Sn [523 K (250 °C)] Needed in Eq. [13]

Symbol	k	c	g	β	ρ	μ
Property	heat conductivity	specific heat	gravitational acceleration	volume expansion coefficient	density	dynamic viscosity
Value	30.68	248.0	9.8	7.374×10^{-5}	6949	2.021×10^{-3}
Unit	W/(m K)	J/(kg K)	m/s^2	K^{-1}	kg/m^3	P_a s

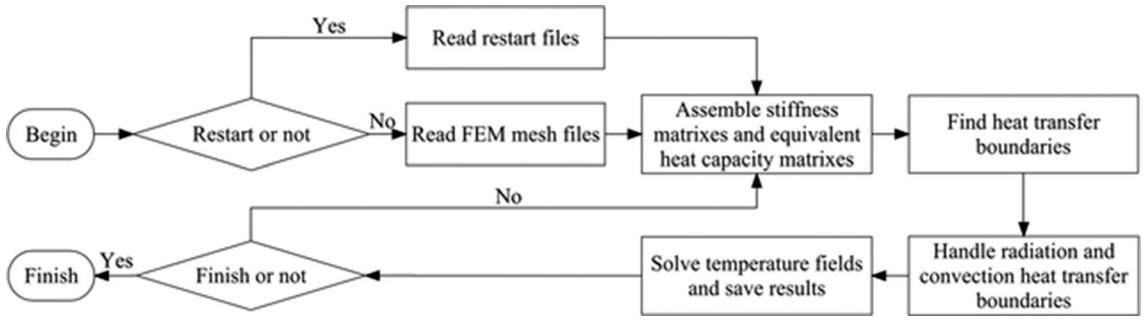

Fig. 2—The solving flow chart of temperature field program in LMC process.

Eqs. [10], [11], and Eq. [12] into Eq. [9], the equivalent heat transfer coefficient h between liquid-metal and solid is as below:

$$h = kC\left(\frac{c^2 g\beta\rho^2}{k(k+c\mu)}\right)^n \Delta T^n L^{3n-1}, \qquad [13]$$

where ΔT is the temperature difference between liquid-metal and solid, K, and L is the depth of solid immersing into liquid-metal, m.

During the experimental process in this paper, the fireproof asbestos was placed on the surface of coolant, and there was stirring device within the coolant, meanwhile, the temperature of coolant was controlled by means of the heating or cooling process with the wall of cooling zone, so the temperature of coolant changed in a small range. Considering that the simulation of the coolant's flow process is quite complicated, the temperature of the coolant is assumed to be constant in this paper.

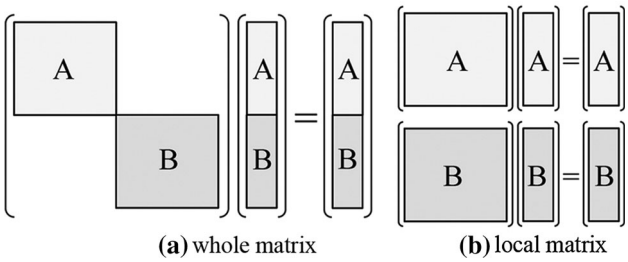

Fig. 3—The schematic diagram of local matrix: (*a*) whole matrix, (*b*) local matrix.

According to Eq. [13], the equivalent heat transfer coefficient h between shell and coolant depends on the physical parameters of coolant, the temperature difference ΔT between shell and coolant and the depth L of shell immersing into the coolant. The liquid-metal coolant of LMC process is liquid Sn [523 K (250 °C)] in this paper, and the physical parameters of liquid Sn [523 K (250 °C)] needed in Eq. [13] are shown in Table I.

By substituting the physical parameters in Table I into Eq. [13], the equivalent heat transfer coefficient h can be determined when the shell gets in touch with the coolant. In the implementation of program, it should be judged dynamically whether the boundary element of shell is immersed into the coolant or not, then the heat transfer coefficient h and the surface emissivity ε of the shell are adjusted to show the transition from radiation to convection, as shown below:

$$\begin{cases} h = 0 & \varepsilon = 0.8 \quad (Z > H) \\ h = 642.6\Delta T^{1/3} & \varepsilon = 0 \quad (Z \le H) \end{cases}, \qquad [14]$$

where Z is the height of boundary element of the shell, m and H is the height of coolant surface, m.

D. *Calculation Methodology*

According to the mathematical model and boundary treatment of LMC process, the solving equation of

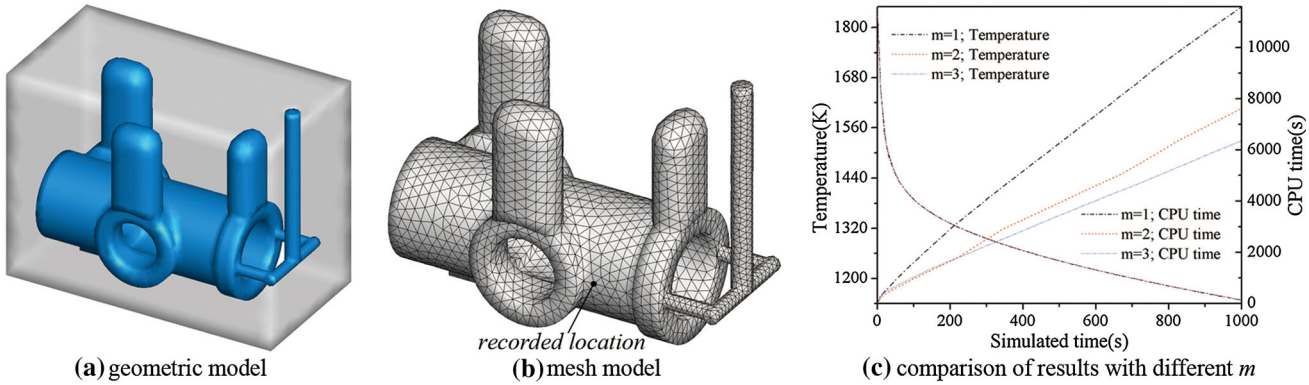

Fig. 4—The effect of mixed time steps on the computational efficiency: (*a*) geometric model, (*b*) mesh model, (*c*) comparison of results with different m.

Table II. The Thermophysical Parameters of CMSX-4 Superalloy Computed by JMatPro

Density		Heat conductivity		Specific heat	
K (°C)	kg/m^3	K (°C)	W/(m K)	K (°C)	J/(g K)
1823 (1550)	7500	1823 (1550)	35.14	1823 (1550)	0.68
1654 (1381)	7650	1654 (1381)	32.18	1538 (1265)	0.60
1602 (1329)	8050	1602 (1329)	35.00	1508 (1235)	0.59
1373 (1100)	8220	1298 (1025)	24.56	1373 (1100)	0.79
1108 (835)	8400	1128 (855)	21.20	1123 (850)	0.62
303 (30)	8700	298 (25)	10.41	313 (40)	0.42

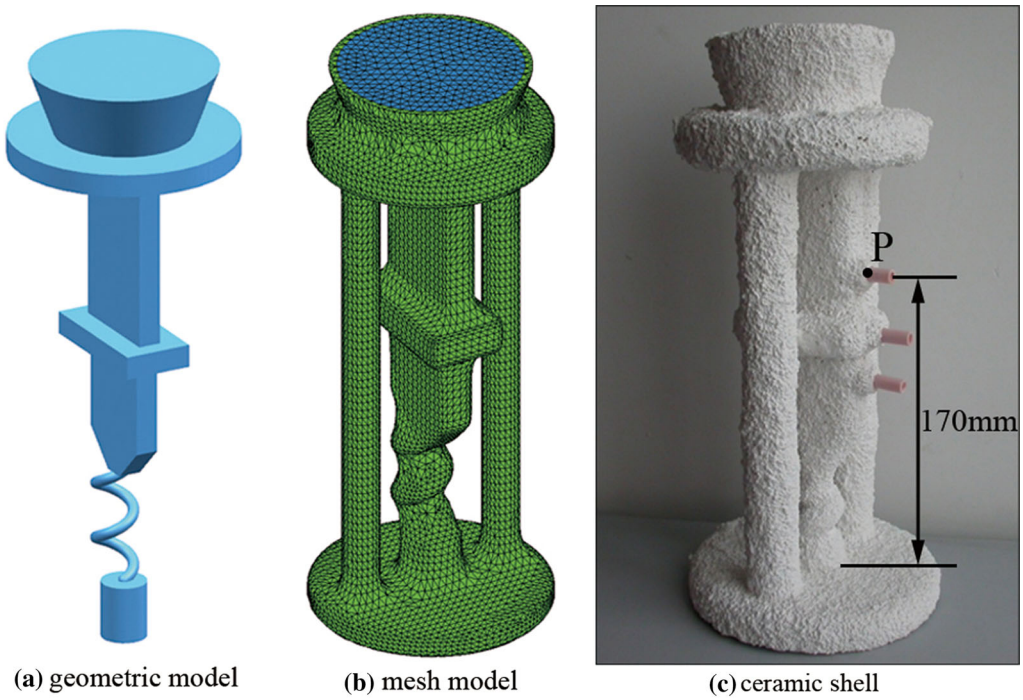

Fig. 5—The casting model and ceramic shell: (*a*) geometric model, (*b*) mesh model, (*c*) ceramic shell.

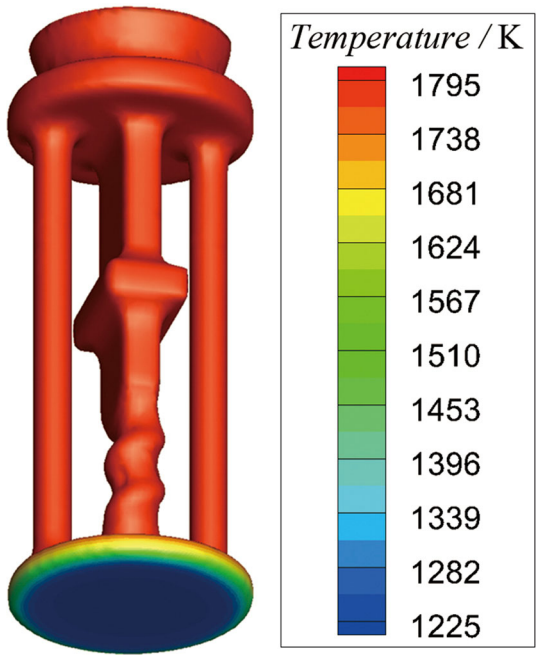

Fig. 6—The preheat temperature field of shell.

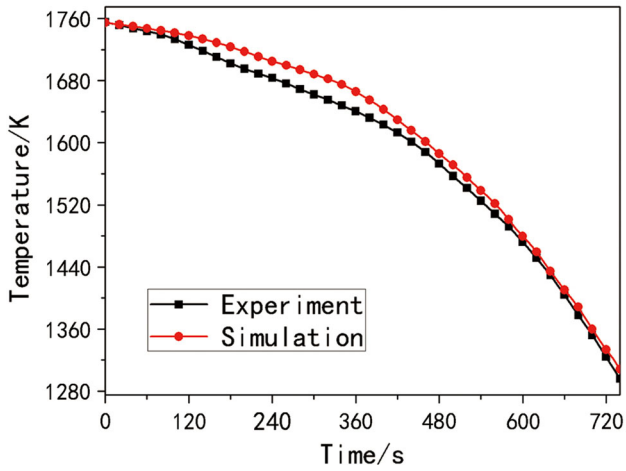

Fig. 7—Comparison of simulation and experiment cooling curve of point P at the withdrawal rate of 6 mm/min.

transient temperature field in LMC process can be described by FEM solving theory,[31] as follows:

$$\boldsymbol{C}\overline{\boldsymbol{T}} + \boldsymbol{K}\boldsymbol{T} = \boldsymbol{N}, \qquad [15]$$

where $\boldsymbol{C}$ is the specific heat matrix, $\boldsymbol{K}$ is the thermal conductivity matrix, $\boldsymbol{N}$ is the load vector, $\boldsymbol{T}$ is the vector of nodal temperature and $\overline{\boldsymbol{T}}$ is the vector of the derivative of nodal temperature with respect to time.

On the base of the compiling environment of Microsoft Visual Studio 2008 (Microsoft Corporation, Redmond, USA), the temperature field numerical simulation program of LMC process based on FEM is developed by the C++ programming language, and the solving flow chart of temperature field program is shown in Figure 2.

Solving matrix operation is required for Eq. [15], and the matrixes in Eq. [15] are supported to contain all the components according to the common idea in FEM, resulting in low computational efficiency with large

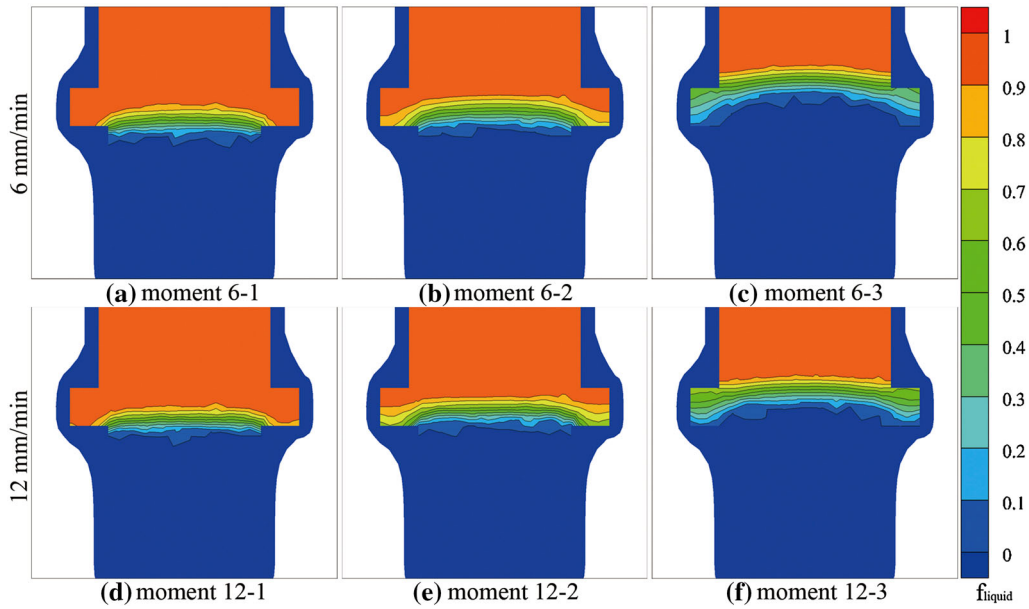

Fig. 8—The shapes of solidification interface and liquid fraction at different withdrawal rates when the interface passing the bottom of platform: (*a*) moment 6-1, (*b*) moment 6-2, (*c*) moment 6-3, (*d*) moment 12-1, (*e*) moment 12-2, (*f*) moment 12-3.

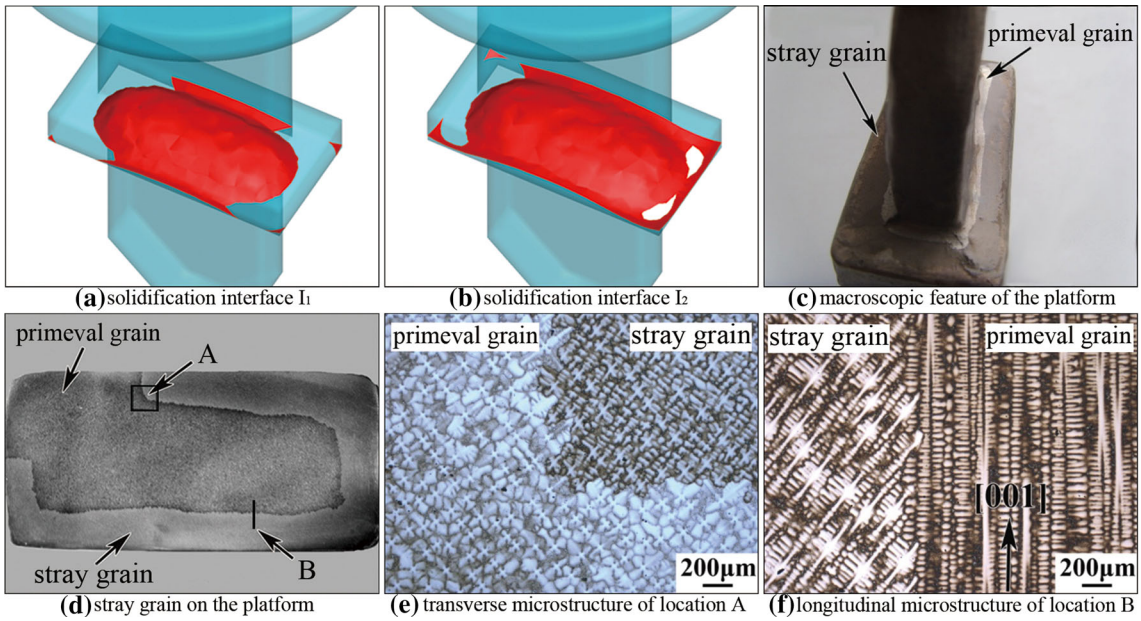

Fig. 9—The analysis of stray grain on the platform at the withdrawal rate of 12 mm/min: (*a*) solidification interface I_1, (*b*) solidification interface I_2, (*c*) macroscopic feature of the platform, (*d*) stray grain on the platform, (*e*) transverse microstructure of location A, (*f*) longitudinal microstructure of location B.

matrixes. Therefore, the concept of local matrix, which means to assemble the matrixes for each component independently, is proposed to raise the computational efficiency. Moreover, the application of local matrix makes it possible to adopt different time steps for different materials. Figure 3 is the schematic diagram of local matrix. The resulting symmetric positive definite systems are solved by preconditioned conjugate gradients[29] method.

In order to verify the feasibility of mixed time step by the application of local matrix, the temperature field of a casting craft is calculated in this paper, and different time steps are set for mold and casting, where *m* is the multiple between the time steps of mold and casting. The temperature changes of a certain location shown in Figure 4b and CPU time under different values of *m*are recorded, as shown in Figure 4c, where all numerical calculations were taken by a desktop

computer with Intel i5-3470 CPU and 4.00 GB RAM. By the comparison of results, mixed time step has a good effect on the computational efficiency, furthermore, the temperature values have no performance difference.

III. RESULTS AND DISCUSSION

A. *The Model of Superalloy Turbine Blade and Parameters Setting*

The alloy material is the nickel-based single crystal superalloy CMSX-4,[36] the chemical compositions of which are 60.68 pct Ni, 6.4 pct Cr, 6.6 pct Ta, 9.6 pct Co, 0.1 pct Hf, 6.4 pct W, 0.61 pct Mo, 5.67 pct Al, 2.9 pct Re, and 1.04 pct Ti. The thermophysical parameters of CMSX-4 superalloy computed by JMatPro software (Sente Software Ltd., Boston, UK) are shown in Table II. The liquidus and solidus temperatures are 1654 K (1381 °C) and 1602 K (1329 °C), respectively, and the latent heat is 101.2 J/g.

The castings of turbine blade in practical production have the complex appearance and hollow internal structure. In consideration of the feasible operation in the experiment, a simplified blade model is chosen here, geometric model of which is shown in Figure 5a. The casting model consists of five parts, including riser, blade, platform, tenon, and grain selector from top to bottom. The mesh model was generated by the tetrahedral grid software of the author's laboratory, and the mesh of shell was obtained on the base of the casting, as shown in Figure 5b. The element and node numbers of the whole mesh model are 140932 and 40156, respectively. It's important to note that the two cylindrical parts of shell play the supporting role.

The LMC equipment with the capacity of 10kg casting was used to produce the blade casting above, which liquid-metal coolant is liquid Sn [523 K (250 °C)], and the ceramic shell adopted in the experiment is shown in Figure 5c. Two withdrawal rates 6 mm/min and 12 mm/min were set in the experiment, and three tests were taken at each withdrawal rate. In order to compare the simulation and experiment results quantitatively, temperature measurement was taken during the experiments under the withdrawal rate 6 mm/min, so a thermocouple which is 170 mm from the baseplate, was placed to measure the temperature of point P on the casting wall, as shown in Figure 5c. The thermocouple wires were put into a ceramic tube, and the joint of ceramic tube was sealed by high-temperature glue, avoiding the access of liquid Sn. The type of thermocouple is W-Re 5/26 (type C). And the temperature was measured by a UJ31 potentiometer, and the data were recorded once per 10 seconds.

B. *Comparison and Analyses for Simulation and Experiment Results*

Before pouring molten metal in the experiment, the shell should be preheated. In the beginning of the program, the mesh model of shell was the only imported component, and the shell was set to be stationary in the heating zone. The radiation information of all the shell boundaries, including the interior, was searched, and the initial temperature of shell was 303 K (30 °C). Then the preheated process of shell was calculated by the program, and the final preheat temperature field was obtained until the temperature field remained stable. Figure 6 shows the final preheat temperature field of shell computed by the program. From the simulation result, the final preheat temperature field presented gradient distribution from the bottom up for the influence of cooling zone, benefiting the formation and directional growth of grain.

The cooling curves of point P in the process of experiment and simulation were recorded at the withdrawal rate of 6 mm/min, shown in Figure 7. By the means of comparing the simulative and experimental temperature data quantitatively, the simulative and experimental temperature values are 1681 K (1408 °C) and 1654 K (1381 °C), respectively, when the temperature difference is the maximum. So the maximum relative error between experiment and simulation cooling curve is 2 pct calculated by the data with unit °C, and experiment and simulation results agree with each other very well. In consequence, the heat transfer model in this paper is suitable for simulating the temperature field of LMC process accurately.

The change of the solidification interface can reflect the situation of grain growth, so the shapes of solidification interface and liquid fraction at different withdrawal rates when the interface passing the bottom of platform are shown in Figure 8. The solidification interface advanced gradually on the bottom of platform at the withdrawal rate of 6 mm/min, so it can be assumed that the single crystal was kept in the process. When the withdrawal rate was increased to 12 mm/min, it can be observed completely that the discontinuous solidification interface occurred, which stands for the generation of stray grain. The analysis of stray grain on the platform at the withdrawal rate of 12 mm/min is shown in Figure 9. Figures 9(a) and (b) show the solidification interface on the bottom of platform, and the isolated solidification interface arose at the corner meaning the appearance of stray grain, which can be seen clearly in Figure 9(c). The macrostructure on the cross section of the platform center is shown in Figure 9(d), besides Figure 9(e) shows the transverse microstructure of location A and Figure 9(f) shows the longitudinal microstructure of location B. From the microstructure results in Figure 9(e) and (f), the orientation of original grain growing from the tenon was [001]. After the stray grain was generated on the corner of platform, the stray grain grew deviated from the orientation [001] and intersected with the original grain in a large angle. The reason for the generation of stray grain on the platform is considered to be that the rate immersing into the coolant increased at the higher withdrawal rate, causing that the both sides of blade cooled faster than the middle obviously and the molten metal at the corner of platform solidified in advance.

IV. CONCLUSIONS

1. The heat transfer model of directional solidification by LMC process based on finite element method was established, and the temperature field numerical simulation program was here developed. The accuracy of the heat transfer model was validated by the cooling curves and grain morphology, and the heat transfer model can be applied to optimize the LMC process effectively.
2. A temperature- and time-dependent heat transfer coefficient was used to represent the heat convection between the shell and the cooling liquid, and an improved Monte Carlo ray-tracing approach was used to handle the boundary of radiation heat transfer. Unstructured mesh was adopted to fit the irregular shell boundary.
3. The concept of local matrix was proposed, in the interest of guaranteeing computational efficiency.
4. The withdrawal rate showed an important influence on the shape of solidification interface, and stray grain is liable to be generated on the bottom of platform at an excessive withdrawal rate.

ACKNOWLEDGMENTS

This research is financially supported by the Program for New Century Excellent Talents in University (No. NCET-13-0229, NCET-09-0396), the National Science & Technology Key Projects of Numerical Control (No. 2012ZX04010-031, 2012ZX0412-011), and the National High Technology Research and Development Program ("863" Program) of China (No. 2013031003).

REFERENCES

1. G.A. Chadwick: *Corros. Eng. Sci. Technol.*, 1984, vol. 19 (4), pp. 154–55.
2. D.X. Ma: *Acta. Metall. Sin.*, 2015, vol. 51 (10), pp. 1179–90.
3. H. Fu and X. Geng: *Sci. Technol. Adv. Mat.*, 2001, vol. 2 (1), pp. 197–204.
4. N. Tang, Y.L. Wang, Q.Y. Xu, X.H. Zhao, and B.C. Liu: *Acta. Metall. Sin.*, 2015, vol. 51 (4), pp. 499–512.
5. C.H. Lund and J. Hockin: *Superalloys*, Wiley, New York, 1972, pp. 403–25.
6. M. Konter and M. Thumann: *J. Mater. Process. Tech.*, 2001, vol. 117 (3), pp. 386–90.
7. J. Zhang, T.W. Huang, L. Liu, and H.Z. Fu: *Acta. Metall. Sin.*, 2015, vol. 51 (10), pp. 1163–78.
8. A.F. Giamei and J.G. Tschinkel: *Metall. Mater. Trans. A*, 1976, vol. 7A (9), pp. 1427–34.
9. J.H. Liu, L. Liu, T.W. Huang, B.M. Ge, J. Zhang, H.Z. Fu, B. Yu, G.Q. Su, P.H. Wang, and X.F. Liu: *Foundry*, 2010, vol. 59 (8), pp. 822–25.
10. A.J. Elliott, S. Tin, W.T. King, S.C. Huang, M.F.X. Gigliotti, and T.M. Pollock: *Metall. Mater. Trans. A*, 2004, vol. 35A (10), pp. 3221–31.
11. A.J. Elliott, G.B. Karney, M.F.X. Gigliotti, and T.M. Pollock: *Superalloys*, TMS, Warrendale, 2004, pp. 421–30.
12. J. Zhang and L.H. Lou: *J. Mater. Sci. Technol.*, 2007, vol. 23 (3), pp. 289–300.
13. G. Liu, L. Liu, X.B. Zhao, W.G. Zhang, T. Jin, J. Zhang, and H.Z. Fu: *Acta. Metall. Sin.*, 2010, vol. 46 (1), pp. 77–83.
14. C.L. Brundidge, D. Vandrasek, B. Wang, and T.M. Pollock: *Metall. Mater. Trans. A*, 2012, vol. 43A (3), pp. 965–76.
15. J.D. Miller and T.M. Pollock: *Metall. Mater. Trans. A*, 2012, vol. 43A (7), pp. 2414–25.
16. R.E. Napolitano and R.J. Schaefer: *J. Mater. Sci.*, 2000, vol. 35 (7), pp. 1641–59.
17. A. Kermanpur, N. Varahram, P. Davami, and M. Rappaz: *Metall. Mater. Trans. B*, 2000, vol. 31 (6), pp. 1293–304.
18. A.J. Elliott and T.M. Pollock: *Metall. Mater. Trans. A*, 2007, vol. 38A (4), pp. 871–82.
19. Y.Z. Lu, D.W. Wang, J. Zhang, and L.H. Lou: *Foundry*, 2009, vol. 58 (3), pp. 245–48.
20. Y.Z. Lu, H.J. Xi, J. Shen, W. Zheng, G. Xie, L.H. Lou, and J. Zhang: *Acta. Metall. Sin.*, 2015, vol. 51 (5), pp. 603–11.
21. X.W. Yan, N. Tang, X.F. Liu, G.Y. Shui, Q.Y. Xu, and B.C. Liu: *Acta. Metall. Sin.*, 2015, vol. 51 (10), pp. 1288–96.
22. A.R. Mitchell and D.F. Griffiths: *The Finite Difference Method in Partial Differential Equations*, Wileys, Hoboken, 1980.
23. H.K. Versteeg and W. Malalasekera: *An Introduction to Computational Fluid Dynamics: the Finite Method*, Pearson Education, New York, 2007.
24. G. Dhatt, E. Lefrançois, and G. Touzot: *Finite Element Method*, Wiley, Hoboken, 2012.
25. G. Vladimir: *Materials in technology*, 2009, vol. 43 (5), pp. 233–37.
26. T. Chen, D.M. Liao, and J.X. Zhou: *Materials Science Forum*, 2013, vol. 762, pp. 224–29.
27. S. Perron, S. Boivin, and J. Hérard: *Comput. Fluids*, 2004, vol. 33 (10), pp. 1305–33.
28. W. Gao, Y.L. Duan, and R.X. Liu: *J. Hydrodyn.*, 2009, vol. 21 (2), pp. 201–11.
29. T. Chen: PhD Thesis, Huazhong University of Science and Technology, 2013.
30. L. Cao, D.M. Liao, L.M. Cao, H.P. Gu, T. Chen, and S.Y. Pang: *Foundry*, 2014, vol. 63 (12), pp. 1235–40.
31. X.C. Wang: *Finite Element Method*, Tsinghua University Press, Beijing, 2003.
32. K. Cui, Q.Y. Xu, J. Yu, B.C. Liu, A. Kimatsuka, Y. Kuroki, and F. Yokoyama: *Acta. Metall. Sin.*, 2007, vol. 43 (5), pp. 465–71.
33. J. Yu, Q.Y. Xu, J.R. Li, H.L. Yuan, S.Z. Liu, and B.C. Liu: *Acta. Metall. Sin.*, 2007, vol. 43 (10), pp. 1113–20.
34. D. Pan, Q.Y. Xu, and B.C. Liu: *Acta. Metall. Sin.*, 2010, vol. 46 (3), pp. 294–303.
35. S.S. Kutateladze and V.M. Borishanskii: *Liquid-Metal Heat Transfer Media*, Consultants Bureau, New York, 1959.
36. X.F. Sun, T. Jin, Y.Z. Zhou, and Z.Q. Hu: *Mater. China*, 2012, vol. 31 (12), pp. 1–11.